

# Simple Mathematical Model for Ferromagnetic Core Inductance and Experimental Validation

B. Nana<sup>1,\*</sup>, S. B. Yamgoué<sup>1</sup>, R. Tchitnga<sup>2</sup>, P. Wofo<sup>3</sup>

<sup>1</sup>Department of Physics, Higher Teacher Training College, University of Bamenda, PO Box 39 Bamenda, Cameroon

<sup>2</sup>Laboratory of Electronics and Signal Processing, Faculty of Science, University of Dschang, PO Box 67 Dschang Cameroon

<sup>3</sup>Laboratory of Modelling and Simulation in Engineering, Biomimetics and Prototypes, Faculty of Science, University of Yaounde I, PO Box 812 Yaounde, Cameroon

\*Corresponding author: [na1bo@yahoo.fr](mailto:na1bo@yahoo.fr), url: <http://www.lamsebp.org>

Received March 02, 2015; Revised March 27, 2015; Accepted April 01, 2015

**Abstract** In determining the properties and inductance of ferromagnetic core inductor, hysteresis modeling is of high importance. Many models are available to investigate those characteristics but they tend to be complex and difficult to implement. In this paper, we report a new mathematical model based on the experimental data of hysteresis for ferromagnetic core inductor. The proposed model can restore the hysteresis curve with a little RMS error. We used the model to determine analytically the expression of the current in a RL series circuit forced by an alternating source. A good agreement is found between our theoretical and experimental results.

**Keywords:** nonlinear, inductance, ferromagnetic, core, hysteresis

**Cite This Article:** B. Nana, S. B. Yamgoué, R. Tchitnga, and P. Wofo, "Simple Mathematical Model for Ferromagnetic Core Inductance and Experimental Validation." *American Journal of Electrical and Electronic Engineering*, vol. 3, no. 2 (2015): 29-36. doi: 10.12691/ajeec-3-2-2.

## 1. Introduction

Magnetic materials are used in electrical power devices such as transformers, motors and generators. They are also present in measurement and control of electrical power for actuators and sensors, contactors and relays. Another application field is found to be in the magnetic recording industry, either by analog or digital, as in audio and video recording or in the storage of data information on magnetic disks and tapes for computer applications. The purpose of a magnetic material core in an inductor is to produce by a given applied field, a higher flux compared to the flux produced in air, and to form a magnetic path for the flux.

In general, all electrical circuit elements respond in a nonlinear fashion to any form of electrical input. However, simple passive elements, such as resistors, capacitors, and air core inductors, respond to a first order approximation nearly linearly. But in devices that have ferromagnetic cores, the relationship between the flux density and the magnetic field strength in the magnetic core is nonlinear. This nonlinear relationship depends on several factors, such as the chemical constitution and structure of the magnetic material, technological process, the way the material is worked and applied. The nonlinear characteristic of the magnetic material is irreversible, hence exhibits hysteresis.

The ferromagnetic cores are basic constructive elements of transformers and inductors for wide application area, ranging from analog and digital microelectronics toward

power converters and power systems. It is known that the rigorous study and design optimization of such electromagnetic devices is difficult because of nonlinearity, electromagnetic inertial behavior and other related phenomena, as saturation, anisotropy, magnetic hysteresis and induced eddy currents.

Hysteresis is a wide research topic in science and engineering. Mathematicians, physicists and engineers have proposed numerous models to describe that phenomenon [1-9]. They are generally fully analytic models based on certain physical theories like Weiss, Preisach or Jiles-Atherton, often restricted to particular applications [10,11,12]. Some apparently accurate models are inadequate when used in circuit simulation because of discontinuities which can provoke severe convergence problems and therefore, alter the simulation results. For many known models used in circuit simulators [13,14], it is difficult to identify the correct correspondence between the model parameters and the real device ones. However, all indicates that this research topic is still far from being fully exploited and that it is difficult to find the ultimate solution and a universal model. This has been and seem to remain a long-term challenge for researchers [15,16].

There are basically three approaches in the modeling of inductance nonlinearity that include hysteresis. The first approach looks at the physical properties of the material: domain alignments, wall movements, spin rotations, etc [17,18]. The second approach prefers a macroscopic description of hysteresis using mathematical models to predict the  $B - H$  curve but without completely neglecting the physics of the material [19]. The third

approach needs the equivalent circuit to be modeled in existing computer programs [20,21].

Thus, the merit of the model developed in this work is that it defines the complex requirements of the particular modeling approach that provides a solution to this problem with excellent accuracy.

The method of analysis used in this research is a combination of direct harmonic domain approach, the Harmonic Balance Method, orthogonalized polynomials and piecewise approximations. It employs the methodology that analyzes the influence of all significant factors in more detail and it includes the representation of hysteresis. The modeling procedure has a wide range of generality, being suitable to be extended to transformers, linear actuators and rotating motors.

The paper is organized as follows: in Section 2, the measurement method is briefly described and the mathematical models are given. Next we analyze the dynamical behavior of a circuit containing a resistor and a ferromagnetic core inductor forced by an alternating generator in Section 3. In Section 4, theoretical and experimental results are presented and the paper is concluded with some remarks in Section 5.

## 2. Measurement Method and Mathematical Models

### 2.1. Measurement Methods

The relation between magnetic induction and magnetic field in ferromagnetism can be presented with a hysteresis loop. Several methods of measurement are commonly applied for the recording of hysteresis loop of ferromagnetic materials, such as Roland's and Juing's method [22] for measuring with direct current, and oscilloscope measuring method which employs AC current.

The AC method requires extensive preparation for the measurement procedure, such as the calibration of the oscilloscope and a proper selection of the components in the secondary electric circuit. In addition, measurement results cannot be stored in an easy and simple way in the proper format. For this measurement, we will use the DC method applied to the connection scheme shown in Figure 1.

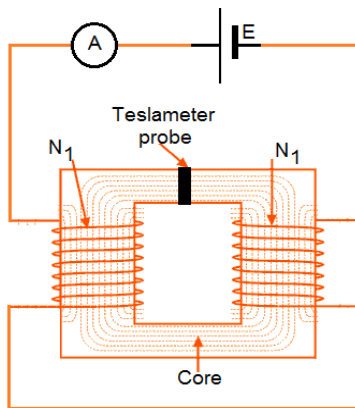


Figure 1. Connection scheme for recording hysteresis loop.

When the current  $I$  measured by the ammeter is proportional to the strength of the magnetic field  $H$ , the

magnetic induction  $B$  is directly measured using a teslameter.

The hysteresis loop we obtained is shown in the graph of Figure 2. It is a three steps illustration. Step one represented by circles corresponds to the variation of the power supply from 0 V to +2 V. Without switching off the circuit, but varying back the power supply from +2 V to -2 V, then forth from -2 V to +2 V, we obtain the second step (triangles) respectively the third depicted by squares.

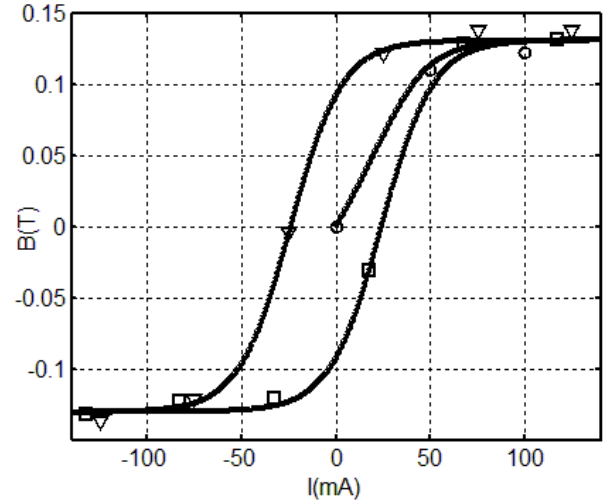


Figure 2. Experimental recorded data (circles, triangles and squares) and splitting (solid line)  $B - I$  curves

### 2.2. Mathematical Model of Hysteresis

Just by considering the shapes of the curves formed by the triangles and squares points, we describe the relation between the magnetic induction and the magnetic field in the following form:

$$B = \mu_0 H + B_s \tanh\left(\frac{\alpha H - \sigma}{2}\right) \text{ with } \sigma = \beta \text{sign}\left(\frac{dH}{dt}\right). \quad (1)$$

$B_s$ ,  $\alpha$  and  $\beta$  are parameters to be determined and the step function  $\text{sign}(x)$  is defined as

$$\text{sign}(x) = \begin{cases} 1 & \text{if } x > 0 \\ 0 & \text{if } x = 0 \\ -1 & \text{if } x < 0 \end{cases} \quad (2)$$

$\mu_0$  is the permeability of free space. One can notice that, for the part of the hysteresis loop with triangles points,  $H$  or  $I$  is decreasing, then  $\sigma = -\beta$  and for the other part,  $H$  is increasing, means that  $\sigma = \beta$ . The relation between magnetic induction and current can be obtained by taking into account the Ampere law:  $H\ell = NI$ , where  $\ell$  is the average length of the magnetic material and  $N = 2N_1$  is the total number of turns. Under this relation, equation (1) becomes

$$B = \frac{\mu_0 NI}{\ell} + B_s \tanh\left(\frac{\alpha NI}{2\ell} - \frac{\sigma}{2}\right) \text{ with } \sigma = \beta \text{sign}\left(\frac{dI}{dt}\right). \quad (3)$$

At this stage, the saturation flux density can be obtained from our recorded data and we found that  $B_s = 130$  mT.

The values of  $\alpha$  and  $\beta$  can be obtained by using the means square method. For the following parameters of our used inductor  $\ell = 24$  cm, the cross sectional area  $A = 176.71$  mm<sup>2</sup> and  $N_1 = 500$  we obtain  $\alpha \simeq 88.22 \cdot 10^{-4}$  m  $\cdot$  A<sup>-1</sup> and  $\beta \simeq 88.42 \cdot 10^{-2}$ . Using these values, the curves we obtained are shown in the graph of Figure 2 with solid line. The results show a good agreement between the experimental values and our mathematical model.

Since ferromagnetic materials are generally characterized by three parameters: the remanence ( $B_r$ ), the coercive magnetic field ( $H_c$ ) and the saturation flux density  $B_s$ , we found general relations between them and the coefficients  $\alpha$  and  $\beta$  in the following form:

$$\alpha = \frac{1}{H_c} \ln \left( \frac{B_s + B_r}{B_s - B_r} \cdot \frac{B_s - \mu_0 H_c}{B_s + \mu_0 H_c} \right), \quad \beta = \ln \left( \frac{B_s + B_r}{B_s - B_r} \right). \quad (4)$$

### 2.3. Mathematical Model of Ferromagnetic Core Inductance

The ferromagnetic core inductance model is obtained through the relation  $\phi = LI = BNA$  where  $A$  is the cross sectional area of the magnetic material and  $\phi$  the magnetic flux through the magnetic material. We then obtain

$$L = \frac{BNA}{I}. \quad (5)$$

Since we have two expressions for  $B$  (see equation (3)), we will use the average of the  $B - I$  curves. Consequently, the inductance of an inductor that contains a ferromagnetic material has the following expression:

$$L = \frac{\mu_0 N^2 A}{\ell} + \frac{B_s NA}{2I} \times \left[ \tanh \left( \frac{\alpha NI}{2\ell} - \frac{\beta}{2} \right) + \tanh \left( \frac{\alpha NI}{2\ell} + \frac{\beta}{2} \right) \right]. \quad (6)$$

For illustration, the experimental result with circles and dashed line and the theoretical result with solid line are plotted in Figure 3.

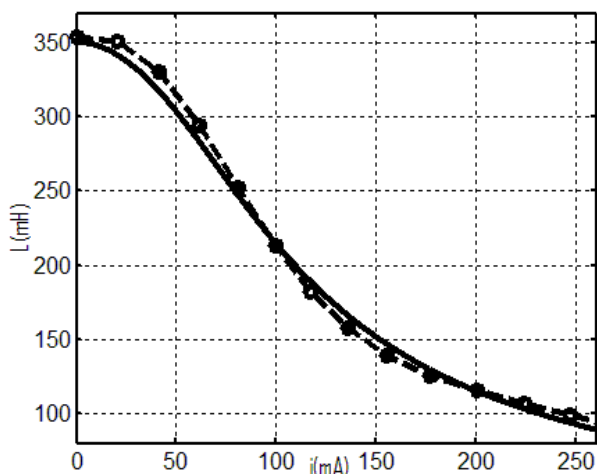


Figure 3. Experimental recorded data (dashed line) and splitting (solid line)  $L - I$  curves.

The experimental values are computed using equation (5) with the recorded values of  $I$  and  $B$ . We have increased the supply voltage from 0V to 2V but the first value of  $I$  we recorded is 1 mA. Also here, there is a good agreement between experimental and theoretical results as the experimental curve fluctuates slightly around the theoretical one.

Regarding the shape of the curve, this result is similar to those obtained experimentally by the authors of references [23,24]. One can also notice from our model that the inductance of a ferromagnetic core inductor lies between two values. The maximum value  $L_i$  and the minimum value  $L_f$  are obtained for very small values of current ( $I = 0$  A) and for infinite values of current respectively. Their expressions are given as follows:

$$L_i = \frac{\mu_0 N^2 A}{\ell} \left[ 1 + \frac{\alpha B_s}{\mu_0 (1 + \cosh \beta)} \right] \text{ and } L_f = \frac{\mu_0 N^2 A}{\ell}. \quad (7)$$

From expressions of  $L_i$  and  $L_f$ , we can deduce the initial relative permeability and the final relative permeability respectively as  $1 + \frac{\alpha B_s}{\mu_0 (1 + \cosh \beta)}$  and 1.

This is a very interesting confirmation of our model since it is known that the relative permeability of a ferromagnetic material is greater than one.

## 3. Dynamics of a Circuit Containing a Resistor in Series with a Ferromagnetic Core Inductor

Since the ferromagnetic core inductance is a function of a current in the circuit and the current is also a function of components in the circuit, the aim of this section is to analyze the dynamics of a circuit where a resistor is connected in series with a ferromagnetic core inductor.

### 3.1. Circuit and Mathematical Model

The circuit diagram is shown on Figure 4, where  $r$  represents the internal resistance of the inductor and  $R_0$  is another resistor added, both to reduce the amplitude of current through the inductor and to measure current.

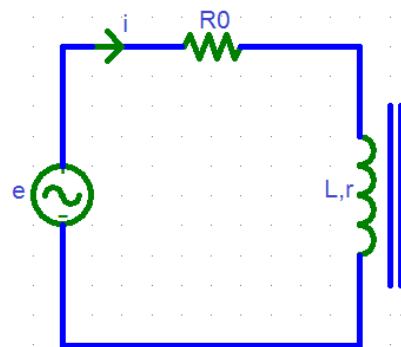


Figure 4. The circuit diagram modeled in this paper.

Since the inductance of such inductor is not constant, the application of the Kirchhoff law leads to the following equation:

$$e = \frac{d(Li)}{dt} + Ri = \frac{d(BNA)}{dt} + Ri. \quad (8)$$

$R = r + R_0$  represents the total resistance of the circuit viewed by the generator. If we replace  $B$  by the corresponding expression as in equation (3) and force the circuit with an alternating generator that has magnitude  $E_m$  and radiant frequency  $\omega$ , we obtain the equation of the circuit as:

$$\left[ \frac{\mu_0 N^2 A}{\ell} + \frac{B_s N^2 \alpha A}{2\ell} \left( 1 - \tanh^2 \left( \frac{\alpha Ni}{2\ell} - \frac{\sigma}{2} \right) \right) \right] \times \frac{di}{dt} + Ri = E_m \sin(\omega t). \quad (9)$$

Here again,  $\sigma$  is defined as in equation (3)

$$\sigma = \beta \text{sign} \left( \frac{di}{dt} \right). \quad (10)$$

Let us define  $t = \frac{\tau}{\omega_0}$  and  $i = I_0 x$  where  $\omega_0$  is a constant and  $I_0 = \frac{\ell}{\alpha N}$ . Then, the state equation (9) can be rewritten in dimensionless form as:

$$g(x)\dot{x} = -\lambda x + E \sin(\Omega \tau) \quad \text{with} \quad (11)$$

$$g(x) = (1-\eta) + \frac{2\eta}{1 + \cosh(x-\sigma)}.$$

The new introduced parameters are defined as follows:

$$\lambda = \frac{R}{L_0 \omega_0}, E = \frac{E_m}{L_0 \omega_0 I_0}, \Omega = \frac{\omega}{\omega_0}, \quad (12)$$

$$\eta = \frac{B_s \alpha}{2\mu_0 + B_s \alpha}, L_0 = \frac{\mu_0 N^2 A}{\ell} \left( 1 + \frac{B_s \alpha}{2\mu_0} \right).$$

### 3.2. Mathematical Analysis

To derive an analytical expression of the current in the circuit, we put the function  $g(x)$  in the form

$$g(x) = \frac{g_1(x)}{g_2(x)} \quad \text{where} \quad g_2(x) = 1 + \cosh(x) \quad \text{and}$$

$g_1(x) = (1+\eta) + (1-\eta)\cosh(x)$ . For simplification, the parameter  $\beta$  is neglected and equation (11) is reduced to:

$$g_1(x)\dot{x} = [-\lambda x + E \sin(\Omega \tau)] g_2(x). \quad (13)$$

Replacing expressions for  $g_1$  and  $g_2$  into equation (13) leads to the following equation:

$$\left[ (1-\eta)\dot{x} + \lambda x - E \sin(\Omega \tau) \right] \cosh(x) = -(1+\eta)\dot{x} - \lambda x + E \sin(\Omega \tau). \quad (14)$$

At this stage, some approximations are needed, we will first expand the function  $\cosh$  in polynomial form as:

$$\cosh(x) = \sum_{m=0}^M \frac{x^{2m}}{(2m)!}. \quad (15)$$

$M$  is the order of the expansion. Equation (14) becomes:

$$(1-\eta) \sum_{m=0}^M \frac{\dot{x} x^{2m}}{(2m)!} + \lambda \sum_{m=0}^M \frac{x^{2m+1}}{(2m)!} + (1+\eta)\dot{x} - E \sum_{m=0}^M \frac{x^{2m}}{(2m)!} \sin(\Omega \tau) = -\lambda x + E \sin(\Omega \tau). \quad (16)$$

For the second approximation, we find the solution in the form  $x = P \cos(\Omega \tau) + Q \sin(\Omega \tau)$  where  $P$  and  $Q$  are unknown parameters to be determined and  $X = \sqrt{P^2 + Q^2}$  represents the magnitude of  $x$ . We obtain after some mathematical transformations the following equation:

$$a\dot{x} + bx - c \sin(\Omega \tau) - (P^2 - Q^2)d \sin(\Omega \tau) = -2PQd \cos(\Omega \tau). \quad (17)$$

The parameters  $a$ ,  $b$ ,  $c$  and  $d$  are defined as:

$$a = (1+\eta) + (1-\eta) \sum_{m=0}^M \left[ \frac{1}{m!(m+1)!} \left( \frac{X}{2} \right)^{2m} \right],$$

$$b = \lambda + \lambda \sum_{m=0}^M \left[ \frac{2m+1}{m!(m+1)!} \left( \frac{X}{2} \right)^{2m} \right],$$

$$c = E + E \sum_{m=0}^M \left[ \frac{1}{(m!)^2} \left( \frac{X}{2} \right)^{2m} \right],$$

$$d = E \sum_{m=1}^M \left[ \frac{1}{(m-1)!(m+1)!} \left( \frac{X}{2} \right)^{2m-2} \right]. \quad (18)$$

Replacing expression for  $x$  into equation (17) and equating the coefficients of  $\sin(\Omega \tau)$  and  $\cos(\Omega \tau)$  in both sides, we obtain the following system:

$$\begin{cases} a\Omega Q + bP = -2dPQ, \\ bQ - a\Omega P = c + d(P^2 - Q^2). \end{cases} \quad (19)$$

After some mathematical manipulations, we obtain the algebraic equation that verifies the amplitude  $X$  as follows:

$$d^4 X^8 + 2cd(b^2 - a^2 \Omega^2 - cd) X^4 + c^4 - d^2(a^2 \Omega^2 + b^2) X^6 - c^2(a^2 \Omega^2 + b^2) X^2 = 0 \quad (20)$$

As the value of  $M$  increases, the power of the above equation also increases. We can derive the analytical solution for two cases  $M = 0$  and  $M = 1$ .

#### 3.2.1. Case $M = 0$

The corresponding equation and the solution are given in equations (21) and (22) respectively.

$$(\lambda^2 + \Omega^2) X^2 = E^2. \quad (21)$$

$$X = \frac{E}{\sqrt{\lambda^2 + \Omega^2}}. \quad (22)$$

In this case, the amplitude of the current and the magnitude of the AC generator are linearly coupled. This

case corresponds to a linear inductor with inductance equals  $L_0$  and is verified for small amplitudes of the current in the circuit. Since we know that as current increases the inductance decreases and the magnetic induction reaches the saturation point.

### 3.2.2. Case $M = 1$

The corresponding equation here is given by relation (23) where the transformation  $Y = X^2$  is used to reduce the order of the algebraic equation.

$$a_3 Y^3 + a_2 Y^2 + a_1 Y + a_0 = 0. \quad (23)$$

The coefficients  $a_3$ ,  $a_2$ ,  $a_1$  and  $a_0$  are defined as follows:

$$\begin{aligned} a_3 &= \lambda^2 + (1-\eta)^2 \Omega^2, a_2 = 32\lambda^2 + 32(1-\eta)\Omega^2 - E^2, \\ a_1 &= 256(\lambda^2 + \Omega^2) - 32E^2, a_0 = -256E^2. \end{aligned} \quad (24)$$

To derive solutions of equation (23), let consider the following parameters:

$$\delta = a_2^2 - 3a_3a_1, q = \frac{2a_2^3 - 9a_3a_2a_1 + 27a_3^2a_0}{2}, \Delta = q^2 - \delta^3.$$

According to the values of parameters, equation (23) can have one or three real solutions and this can be decided through the sign of  $\Delta$ .

If  $\Delta > 0$ , equation (23) has one real solution from which we can deduce the amplitude of the normalized current as:

$$X = \left[ \frac{-a_2 + \sqrt[3]{q - \sqrt{\Delta}} + \sqrt[3]{q + \sqrt{\Delta}}}{3a_3} \right]^{1/2}. \quad (25)$$

If  $\Delta < 0$ , equation (23) has three real solutions and the corresponding expressions of  $X$  are given a follow:

$$\begin{aligned} X_1 &= \left( \frac{-a_2 + 2\sqrt{\delta} \cos\left(\frac{\theta - 2\pi}{3}\right)}{3a_3} \right)^{1/2}, \\ X_2 &= \left( \frac{-a_2 + 2\sqrt{\delta} \cos\left(\frac{\theta}{3}\right)}{3a_3} \right)^{1/2}, \\ X_3 &= \left( \frac{-a_2 + 2\sqrt{\delta} \cos\left(\frac{\theta + 2\pi}{3}\right)}{3a_3} \right)^{1/2} \end{aligned} \quad (26)$$

where  $\theta = \arctan\left(\frac{\sqrt{-\Delta}}{q}\right)$ .

Even if the analytical method gives more than one solution, we think that for the stability of the circuit the appropriate solution is the one with smallest amplitude. According to this fact, we can say that the required value of  $X$  is the minimum value between  $X_1$ ,  $X_2$  and  $X_3$ .

## 4. Results and Comparisons

The aim of this subsection is to present our theoretical and experimental results and give comparison between them. The experimental values are  $r = 4.0 \Omega$ ,  $R_0 = 10 \Omega$ ,  $\ell = 24$  cm,  $A = 176.71$  mm<sup>2</sup> and  $N = 1000$ .  $E_m$  and  $\omega = 2\pi f$  are used as control parameters with  $0V \leq E_m \leq 30V$  and  $10 \text{ Hz} \leq f \leq 250 \text{ Hz}$ . The corresponding theoretical values computed using equation (12) worth:  $\lambda = 66.2 \cdot 10^{-4}$ ,  $\eta = 0.9978$ ,  $L_0 = 423.18$  mH,  $\omega_0 = 5 \cdot 10^3$  rad/s and  $I_0 = 27.2$  mA.

### 4.1. Effect of the Amplitude $E_m$

For our first investigation, we will maintain constant the frequency at  $f = 50$  Hz ( $\Omega = 0.0628$ ), then record the amplitude of the current as  $E_m$  is increasing. Our analytical and numerical results are shown on the graphs of Figure 5.

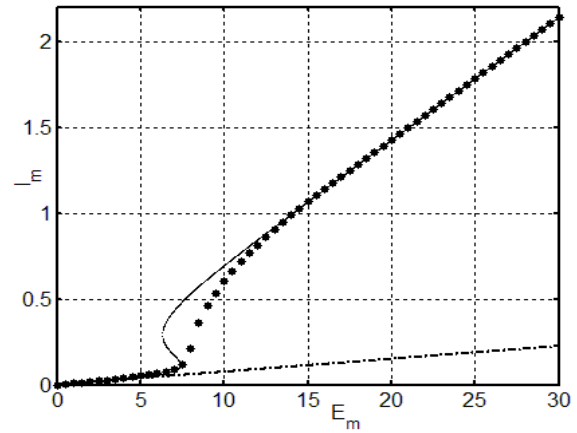


**Figure 5.** Amplitude of the current  $I_m$  versus the magnitude of the external generator  $E_m$ : Numerical obtained (curve with dots), first order (dashed line) and second order (solid line) analytical plotted

The curve with dashed line is obtained by using equation (22) while the curve with full line is obtained from equation (25) or (26). The curve with dots represents our numerical results obtained by solving directly the differential equation (11) with the fourth order Runge Kutta method.

As the graph reveals, the result obtained analytically with the first order approximation ( $M = 0$ ) agrees with the numerical ones just for small values of  $X_m = X \cdot I_0$ . As we mentioned above, the first order approximation (linear approximation) is valid for small amplitudes of current. One can note the good agreement between results obtained analytically with the second order approximation ( $M = 1$ ) and the numerical ones. A small disagreement is found when  $E_m$  is around 8V and we think that this can be overcome by increasing the approximation order.

Figure 6 depicts the comparison between our numerical results (curve with full line) and the experimental results (curve with dots).

Here, it can also be noticed that, the experimental results agree with the numerical ones and consequently with the analytical results obtained from the second order approximation.

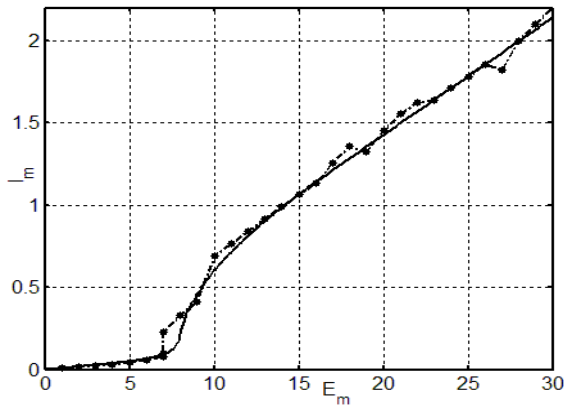


**Figure 6.** Amplitude of the current  $I_m$  versus the magnitude of the external generator  $E_m$  : Numerical obtained (solid line) and experimental recorded (dots and dashed lines)

Even in the case of high amplitudes of current and high amplitudes of the external generator, a good agreement remains between the numerical and analytical results as shown in the graph of Figure 7. Here, the frequency of the external generator equals 200 Hz and we plot the amplitude of the current  $I_m$  versus the magnitude of the external generator  $E_m$ . Also here, a small disagreement is found when  $E_m$  is around 35V and we think that this can be overcome by increasing the approximation order.

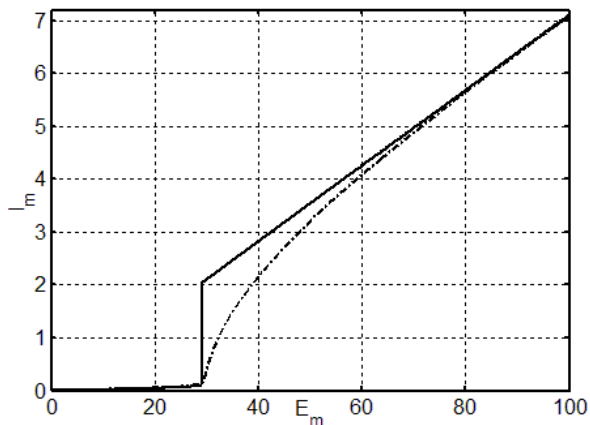
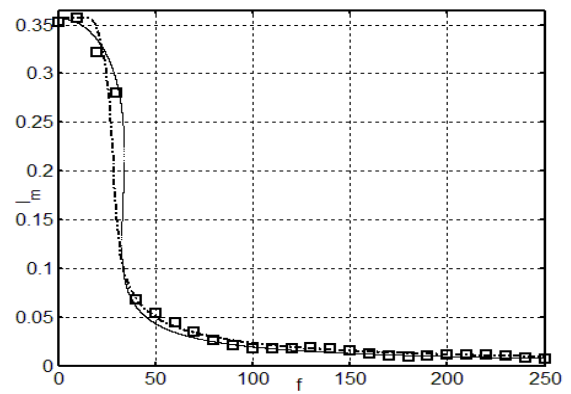


**Figure 7.** Amplitude of the current  $I_m$  versus the magnitude of the external generator  $E_m$  : Numerical obtained (dashed line) and analytical plotted (solid line)

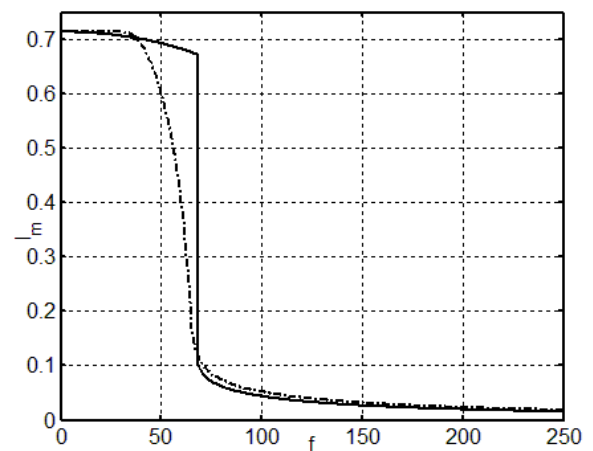
#### 4.2. Effect of the Frequency $f$

In this step, the magnitude of the external AC signal is kept constant and we analyze the effect of the frequency using the second order approximation for our analytical treatment. The graph of Figure 8 obtained for  $E_m = 5$  V shows the comparison between the numerical results (curve with dashed line), the analytical results (curve with full line) and the experimental results (curve with squares). It can be observed that the three results are slightly identical and the shape of the curves is similar to that of the low pas filter obtained in the classical RL circuit.

Also here and as mentioned in the previous section, we found a small disagreement between analytical and numerical results when the frequency is located around 60 Hz and  $E_m$  around 8 V. For illustration, using  $E_m = 10$  V we obtained the curves shown in Figure 9.



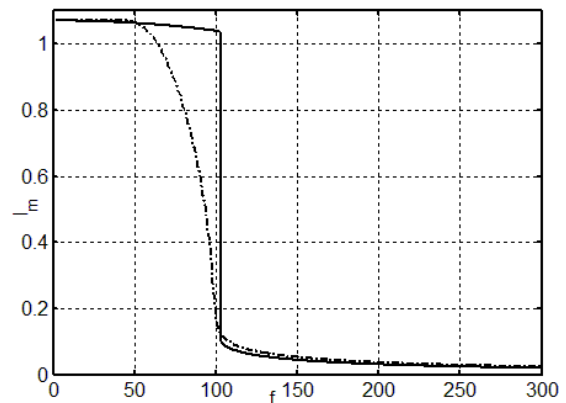
**Figure 8.** Amplitude of the current  $I_m$  versus the frequency of the external generator  $f$  : Comparison between the numerical (dashed line), the analytical (solid line) and the experimental results (dots) with  $E_m = 5$  v.



**Figure 9.** Amplitude of the current  $I_m$  versus the frequency of the external generator  $f$  : Comparison between the numerical (dashed line) and the analytical (solid line) results with  $E_m = 10$  v.

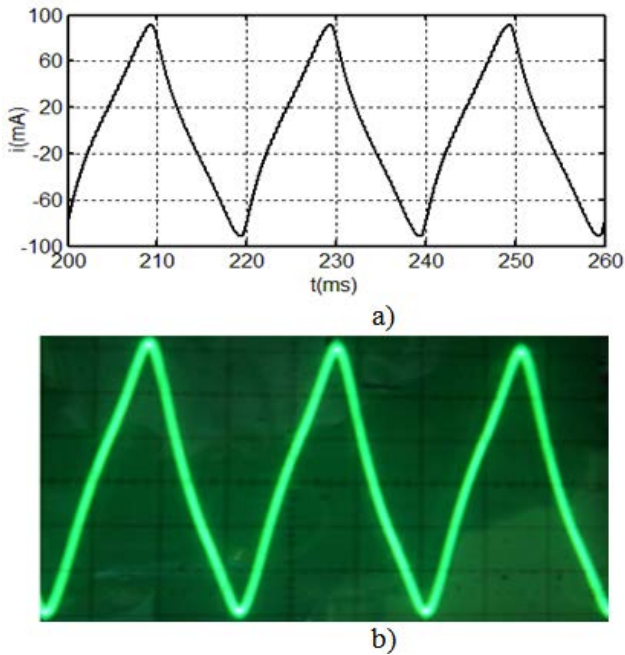
The numerical results (dashed line) and the analytical results (full line) are slightly different in a certain frequency range.

Figure 10 highlights the comparison between our numerical results (curve with dashed lines) and the analytical results (curve with full line) when the magnitude of the external force is increased at  $E_m = 15$  V. Qualitatively, Figure 9 and Figure 10 have the same behavior and hence the same comments.



**Figure 10.** Amplitude of the current  $I_m$  versus the magnitude of the external generator  $E_m$  : Numerical obtained (solid line) and experimental recorded (dots and dashed lines).

The numerical simulations of equation (11) give results that agree well with those obtained experimentally (see Figure 11 and Figure 12) for  $E_m = 5$  V and  $E_m = 9$  V with  $f = 50$  Hz



**Figure 11.** Time waveforms of the current obtained for  $f = 50$  Hz and  $E_m = 7$  V. a) Numerically plotted and b) obtained experimentally

Figure 11a) and Figure 12a) are obtained numerically while Figure 11b) and Figure 12b) are their experimental corresponding.

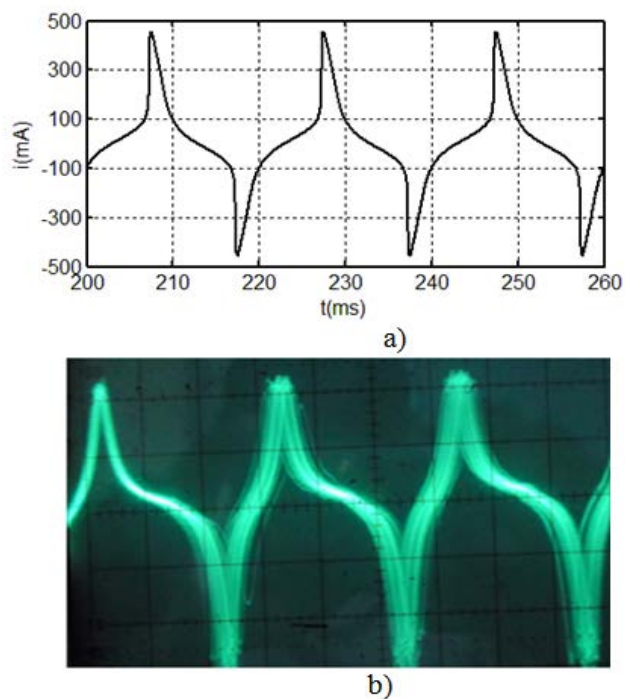


**Figure 12.** Time waveforms of the current obtained for  $f = 50$  Hz and  $E_m = 9$  V. a) Numerically plotted and b) obtained experimentally

On the other hand even if the shape of the current does not respect the sinusoidal form, the amplitudes obtained from the mathematical analysis can be compared to the experimental ones.

## 5. Conclusion

As far the authors are aware, the circuit of Figure 4 has not until now been modeled in a way that includes the ferromagnetic materials parameters and hysteresis. Our model has been incorporated into the differential equation that describes the circuit and has been shown to be able of displaying all the behavior observed in experiment. Another advantage of our model is that the analytical treatment can now be done to predict the amplitude of the current through a ferromagnetic core inductor. We found here a good agreement between the numerical and experimental results as well as our analytical results.

Our next investigation is to test this model on various soft and hard magnetic materials used in industrial devices. We think also that the analysis of the high frequencies effect on the accuracy of this model is another good idea. The study of electrical transformers and motors using this model is a further interesting subject.

## References

- [1] Visintin, A. *Differential Models of Hysteresis*, Applied Mathematical Science, Springer-Verlag, New York, 1994.
- [2] Górecki, K. and Zarobski J, "Modelling of Inductors and Transformers in SPICE," *Elektronika - konstrukcje, technologie, zastosowania, Not-Sigma*, 1(2). 40-43. 2004.
- [3] Górecki, K, "SPICE-aided Modelling of Coils with the Ferrite Core with Selfheating Taken into Account," *Kwartalnik Elektroniki i Telekomunikacji*, 3(5). 389-404. 2003.
- [4] Chiesa, N. and Hoidalén, H.K, "Modeling of nonlinear and hysteretic iron-core inductors in ATP," in *EEUGMeeting 2007*, European EMTP-ATP Conference, Leon, Spain, Sep. 2007.
- [5] Anderson, J.C, *Magnetism and Magnetic Materials*, Champen and Hall Ltd. London, 1968.
- [6] Chua, L.O. and Stromsmoe, K.A, "Lumped-Circuit Models for Nonlinear Inductors Exhibiting Hysteresis Loops," *IEEE Transactions on Circuit Theory*, 17(4). 564-574. Nov. 1970.
- [7] Carnevale, D., Nicosia, S. and Zaccarian, L, "Generalized Constructive Model of Hysteresis," *IEEE Transactions on Magnetics*, 42(12). 3809-3817. Dec. 2006.
- [8] Chua, L.O. and Bass, S.C, "A Generalized Hysteresis Model," *IEEE Transactions on Circuit Theory*, 19(1). 36-48. Jan. 1972.
- [9] Chiesa, N., Avendano, A.H., Hoidalén, K., Mork, B.A., D. Ishchenko, D. and Kunze, A.P, "On the ringdown transient of transformers," in *IPST'07 - International Conference on Power System Transients*, Lion, France, (229). 4-7. Jun. 2007.
- [10] Jiles, D.C. and Atherton D.L, "Ferromagnetic Hysteresis," *IEEE Transactions on Magn.* 19(5). 2183-2185. Sep. 1983.
- [11] Fiorillo F. and Dupré L.R, "Comprehensive Model of Magnetization Curve, Hysteresis Loops, and Losses in Any Direction in Grain-Oriented Fe-Si," *IEEE Transactions on Magn.* 38(3). 1467-1476. Jun. 2002.
- [12] Carnevale D., Nicosia S. and Zaccarian L, "Generalized Constructive Model of Hysteresis," *IEEE Transactions on Magn.* 42(12). 3809-3817. Dec. 2006.
- [13] Brachtendorf H.G., Eck C. and Laur R, "Macromodeling of Hysteresis Phenomena with SPICE," *IEEE Transactions on Circuits and Systems - II: Analog and Digital Signal Processing*, 44(5). 378-388. May. 1997.
- [14] Chan J.H., Vladimirescu A., Gao X.C., Liebmann P. and Valainis J, "Nonlinear Transformer Model for Circuit Simulation," *IEEE Transactions on Computer-Aided Design*, 10(4) 476-482. Apr. 1991.
- [15] Germain, N., Maestero, S. and Vroman, J, "Review of Ferroresonance Phenomena in High Voltage Power Systems and Presentation of a Voltage Transformer Model for Predetermining Them," *CIGRE*, 33-18.1972.
- [16] Nakra, H.L. and Barton, T.H, "Three Phase Transformer Transients," *IEEE Transactions on Power Apparatus and Systems*, 93(1). 1810-1819. Nov./Dec. 1974.

- [17] De Leon, F. and Semlyn, A, "A Simple Representation of Dynamic Hysteresis Losses in Power Transformer," *IEEE Transactions On Power Delivery*, 10(1). 315-321. Jan. 1995.
- [18] Wright, A. and Carneiro, S, "Analysis of Circuits Containing Components with Cores of Ferromagnetic Material," *IEE Proceedings*, 121(12). 1579-1581. Dec. 1974.
- [19] Greene, J.D. and Grass, A.C. "Nonlinear Modeling of Transformer," *IEEE Transactions on Industry Applications*, 24(3). 434-438. Jun. 1988.
- [20] Yamada, S., Besho K. and Lu, L, "Harmonic balance finite element method applied to the nonlinear AC magnetic analysis," *IEEE Trans. On Magn.* 25(6). 2971-2973. Jul. 1989.
- [21] Huang, S.R., Chung, S.C., Chen B.N. and Chen, Y.H, "A Harmonic Model for the Nonlinearities of Single-Phase Transformer with Describing Function," *IEEE Transaction On Power Delivery*, 18(3). 815-820. Jul. 2003.
- [22] Radmanesh, H., Abassi, A. and Rostami, M, *Analysis of Ferroresonance Phenomena in Power Transformers Including Neutral Resistance Effect*, IEEE conference, Georgia, USA, 2009.
- [23] Gianduzzo, J.C. Ygorra, S. and Lasne. L, « La ferrorésonance, experimentation, et modélisation non linéaire, » Université de Bordeaux 1, Centre de Ressource en EEA.  
<http://ferroresonance.free.fr>.
- [24] Salas, R.A. and Pleite, J, "Simple Procedure to Compute the Inductance of a Toroidal Ferrite Core from the Linear to the Saturation Regions," *Materials*, 6(3). 2452-2463. Jun. 2013.